Effects of isotope doping on the phonon modes in graphene

by

Joaquin F. Rodriguez-Nieva

Submitted to the Department of Materials Science and Engineering
in partial fulfillment of the requirements for the degree of

Master of Science

at the

MASSACHUSETTS INSTITUTE OF TECHNOLOGY

September 2012

Author .....
Department of Materials Science and Engineering
August 6, 2012

Certified by .....
Mildred S. Dresselhaus
Professor
Thesis Supervisor

Certified by .....
Silvija Gradečak
Thesis Reader

Accepted by .....
Gerbrand Ceder
Chairman, Departmental Committee on Graduate Students

Effects of isotope doping on the phonon modes in graphene

by

Joaquin F. Rodriguez-Nieva

Submitted to the Department of Materials Science and Engineering
on August 6, 2012, in partial fulfillment of the
requirements for the degree of
Master of Science

Abstract

Carbon related systems have attracted a large amount of attention of the science and technology community during the last few decades. In particular, graphene and carbon nanotubes have remarkable properties that have inspired applications in several fields of science and engineering. Despite these properties, creating structurally perfect samples is a difficult objective to achieve. Defects are usually seen as imperfections that degrade the properties of materials. However, defects can also be exploited to create novel materials and devices. The main topic of this thesis is studying the effect of isotope doping on the phonon properties of graphene. The advantage of the isotope enrichment technique is that only phonon frequencies or thermal properties can be modified without changing the electrical or chemical properties. We calculated the values of the phonon lifetimes due to isotope impurity scattering for all values of isotopic fractions, isotopic masses and for all wavevectors using second order perturbation theory. We found that for natural concentrations of ^{13}C, the contribution of isotopic scattering of optical modes is negligible when compared to the contribution from the electron-phonon interaction. Nevertheless, for atomic concentrations of ^{13}C as high as $\rho = 0.5$ both the isotopic and electron-phonon contributions become comparable. Our results are compared with recent experimental results and we find good agreement both in the ^{13}C atomic density dependence of the lifetime as well as in the calculated spectral width of the G-band. Due to phonon scattering by ^{13}C isotopes, some graphene phonon wavefunctions become localized in real space. Numerical calculations show that phonon localized states exist in the high-energy optical phonon modes and in regions of flat phonon dispersion. In particular, for the case of in-plane optical phonon modes, a typical localization length is on the order of 3 nm for ^{13}C atomic concentrations of $\rho \approx 0.5$. Optical excitation of phonon modes may provide a way to experimentally observe localization effects for phonons in graphene.

Thesis Supervisor: Mildred S. Dresselhaus
Title: Professor

Acknowledgments

I would like to thank my supervisor Prof. Mildred S. Dresselhaus for all her teachings which have helped me not only to obtain scientific results, but also to collaborate with scientists overseas and to communicate science accurately in oral and written forms. I thank Prof. Riichiro Saito for teaching me new physics, for having stimulating discussions with me and for being the main collaborator in this project and, hopefully, in many others to come. Additionally I would like to thank the members of the MGM group for their support, including Dr. Gene Dresselhaus, Laura Doughty, Read Schusky, Paulo Araujo and former members Mario Hofmann and Xiaoting Jia. I would also like to thank Prof. Jing Kong and her group for giving me the possibility of discussing experimental research with them. Last but not least, I thank my parents and brothers for their constant support and encouragement.

Contents

List of Figures

Chapter 1

INTRODUCTION

Carbon related systems have had a large impact on science and technology in the last few decades. Because carbon atoms are bonded together by covalent bondings and due to the low atomic number, the carbon-carbon bond is one of the strongest chemical bonds found in nature. The carbon orbitals hybridize in many different forms such as sp^1, sp^2, sp^3, etc., and as a consequence, carbon is naturally present in many allotropic forms. The initial work done on three-dimensional graphite was later extended to zero-dimensional fullerenes and one-dimensional nanotubes. More recently, the interest in carbon related systems has increased exponentially since individual layers of graphite, called graphene, were individually isolated [5] forming a novel two-dimensional system. This novel nano-material has extraordinary electrical, optical, thermal and mechanical properties and for this reason numerous applications in a large variety of fields are being studied. Among them we can mention graphene as a ballistic transistor [6, 7], sensor [8, 9, 10], electrode [11] and coating [12]. At the same time, in addition to these, carbon nanotubes [13], which can be understood as a rolled sheet of graphene, can be used as a structural material [14, 15].

Even though large samples of graphene can be produced with high purity, the presence of defects is very difficult to avoid. In fact, because graphene is two-dimensional, long-range carbon order is only possible at zero temperature (Hohenberg-Mermin-Wagner theorem [16]). At finite temperatures, topological defects such as dislocations are always present. Although defects can be seen as imperfections in the material

that can degrade its properties, defects can actually be used to generate novel devices. Understanding from a fundamental point of view the effect of defects on these nanomaterials is a first step towards this goal. At the same time, the fact that carbon nanotubes and graphene are one and two-dimensional systems, respectively, allows us to study defects in a different setting than what is conventionally done (i.e., in 3-D). As an example, dislocations, which can be seen as line defects in a 3-D material, can become less intuitive in lower dimensions [17].

1.1 Basic Properties and Applications

Graphene is a single layer of carbon atoms in an hexagonal lattice. Atoms hybridize with sp^2 bondings and the π-bonds are mostly responsible for its electronic properties. Graphene has no band gap but the electronic density of states vanishes at the Fermi level. The electronic dispersion relation is linear in E vs. k at the corners of the Brillouin zone (BZ), also called Dirac cones (see Fig. 1-1(a)) and can be described as $E_k = v_F|k|$, where $v_F = 10^6$ m/s is the Fermi velocity and k is the wavevector with respect to the K-point. Therefore, the effective mass of the electrons at the Dirac point is zero, leading to interesting electronic properties. The electron mobility is remarkably high, in excess of 15000 cm^2/Vs [18]. From a fundamental point of view, interesting physics occurs in this system, such as the anomalous Quantum-Hall effect [19], surface enhanced Raman spectroscopy (SERS) [20, 21] and remarkable spin transport phenomena [22].

The thermal conductivity of graphene at room temperature is on the order of 4000 W/mK [23], which is remarkably high as in other carbon systems like carbon nanotubes and diamond. The phonon dispersion relations are plotted in Figure 1 (b). Similarly, their mechanical properties make graphene and carbon nanotubes one of the strongest materials known, achieving a Young Modulus of approximately 0.5 TPa [24].

Several applications can exploit the properties of graphene. From a technological point of view, some of the most interesting properties are the high mobility, me-

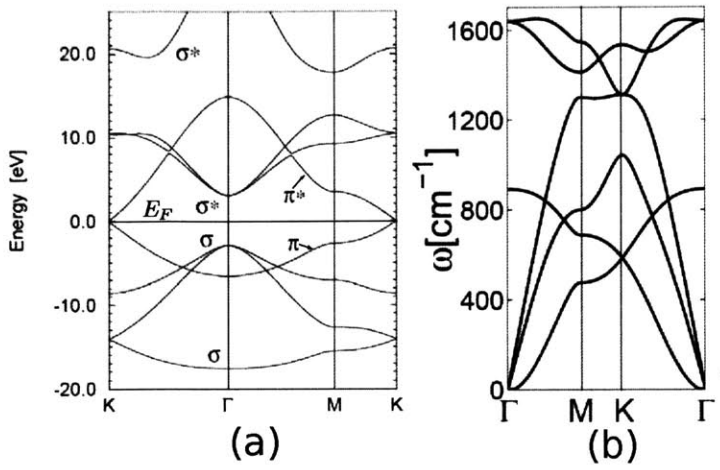

Figure 1-1: (a) Graphene electronic band structure for π and σ bands and (b) phonon dispersion relations [1].

chanical and electrical resilience [25], absence of back-scattering [26] and high crystal quality [25]. Graphene has great potential in high-speed and high-frequency electronics, achieving operating frequencies of 300 GHz [7]. The high carrier mobility, tunable band-gap, ballistic transport and transparency make graphene ideal for optoelectronic devices. Some of the applications based on this aspect are touch-screens, light-emitting diodes and solar cells. Because graphene has a low electronic noise, graphene is highly sensitive to chemical species and this can be exploited in sensors. Individual gas molecules can be detected [8] and, additionally, graphene can also be used when high sensitivity to electrical charge, magnetic fields and mechanical strain are required. Because of its small thickness, graphene can also be used as an electrode material for capacitors [27] in rechargeable batteries, for instance.

1.2 Types of Defects

1.2.1 Edges

As in every crystal structure, graphene has boundaries (also called edges) which are one-dimensional. The high-symmetry edges are the armchair and the zig-zag edge which have different symmetries from one another (Fig. 1-2). In the context of

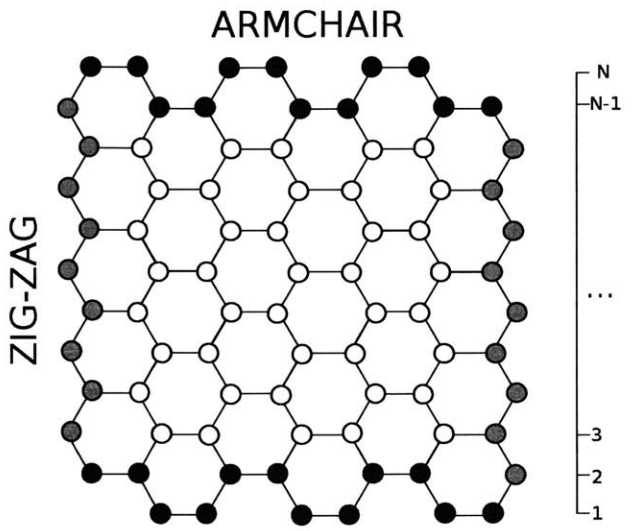

Figure 1-2: Zig-zag and Armchair edges in graphene.

carbon nanotubes, unzipped nanotubes form graphene nanoribbons. The process of unzipping has been developed in the last few years [28]. Elementary calculations using tight-binding approaches show that the type of edge influences whether the material is metallic or semiconducting. Armchair graphene nanoribbons (AGNR) can be both metallic (only when N=3M-1, with M an integer and N defined as in Fig. 1-2) or semiconducting depending on the width of the nanoribbon, but all zig-zag graphene nanoribbons (ZGNR) are metallic, with a high density of electronic states at the edges. Moreover, ZGNR are more reactive than AGNR [29, 30]. This shows that properties that seem to be unrelated to the electronic transport such as the nature of the edge, can have an important effect on the properties of the nanoribbon. Optical techniques like Raman spectroscopy can be used to characterize graphene nanoribbons at the moment of fabrication. With more elaborate calculations, it is found that all nanoribbons have an energy gap [31], but in the case of ZGNR, the gap is a minigap of the order of a few meV.

For electronic applications, it is necessary to open a gap on the order of a few hundred meV. Calculations show that increasing the ribbon width decreases the gap and therefore, it would be necessary to decrease the dimensions of the ribbon to the nanoscale for realistic calculations. Functionalizing edges for chemical applications

is also another area of research. Edges can also produce magnetism in nanoribbons, which can also have potential applications in spintronics [22].

1.2.2 Vacancies

The presence of vacancies create disconnection between atoms. In perfect graphene, each carbon atom bonds with three other carbon atoms. Ion irradiation can produce vacancies in graphene [32]. As in three dimensional structures, vacancies will produce a distortion of the lattice in non-trivial ways. In the case of graphene, we can find different structures such as vacancies, di-vacancies, tri-vacancies and Thrower-Stone-Wales (TSW) defects (Fig. 1-3). Further theoretical work on the generation of vacancies needs to be done. Experimental work that can elucidate the effect of vacancies can be done using TEM. In addition to changing the basic properties of graphene, these sites can be functionalized with different atoms or molecules for specific sensor devices.

1.2.3 Topological defects

Topological defects do not change the connectivity of carbon in the lattice, but they produce changes in the physical properties. Among defects we can include heptagon-pentagon dislocations, Thrower-Stone-Wales (TWS) defects (see Fig. 1-3), double pentagon-octagon, double heptagon-pentagon, grain boundaries and extended line of defects [33].

The main effect of the TWS transformation is a 90° rotation of a bond preserving connectivity and producing no dangling bonds [34]. Theoretical work has been done to create lattices which, in addition to hexagons, also have pentagons and heptagons in either a local way or in an ordered way (for instance, like in Haeckelites [35]). This becomes a geometrical problem in which an ordered arrangement has to be constructed to form more complicated structures. For instance, it has been shown through TEM imaging that in low angle grain boundaries these complex structures are formed. Even though this is the simplest way to create a topological defect, other

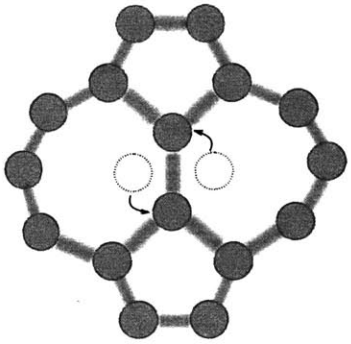

Figure 1-3: Construction of a Thrower-Stone-Wales (TSW) defect. One C-C bond is rotated by 90° to form two pentagons and two heptagons.

types of structures have been proposed like 8-5-8 structures, T5T7 structures, etc. These defects are reactive and can be used to trap atoms or molecules. Inclusion of these defects in the study of properties has been done in thermal transport [36], chemical functionalization [37], mechanical properties [38] and electronics [39, 40, 41].

1.2.4 Substitutional Atoms

Chemical, electronic and thermal properties of graphene can be modulated in a controlled manner by substitutional doping. Atoms in the hexagonal lattice are substituted by dopants (N, B, P, etc.) that disrupt the sp^2 hybridization and cause changes in the band structure as well as an enhancement of specific properties. Graphene can be functionalized and such a material can, for instance, be used in sensors. Dopants can induce an opening of band gaps and achieve a metal-semiconducting transition. For this purpose, theoretical work was done on nitrogen [42], boron [43, 44], sulfur [45] and silicon [46] doping, achieving band gaps of up to 0.6 eV. Another way of doping graphene is to modulate the thermal properties without altering the electronic properties, and this is achieved by ^{13}C isotope doping [47]. This effect is the main topic of this thesis.

1.3 Outline

The outline of this thesis is as follows. In Chapter 2, the fundamentals of Raman spectroscopy will be introduced in order to understand the general context of the present work. Additionally, the physics of phonons is reviewed and the methods that were used to calculate the important quantities are described. In Chapter 3 we present the results of the phonon lifetime calculations as well as phonon localization effects [2]. In Chapter 4 we present the conclusions of this thesis and future work.

Chapter 2

THE PHYSICS OF PHONONS AND RAMAN SPECTROSCOPY

2.1 Fundamentals of Raman Spectroscopy

When shining light on to a material, part of the photon beam is transmitted, while the rest interacts with the material causing absorption, reflection, light scattering and photoluminescence. The exact way in which this interaction occurs depends on the details of both the electronic and the vibrational properties of the material. Therefore, light scattering techniques can be used to probe the fundamental excitations of molecules and solids.

When light scatters inelastically, the energy of the incident light will be different from the energy of the outgoing light, and this energy difference can be measured experimentally. The inelastic scattering of light is called the Raman effect. Figure 2-1 shows a typical Raman spectra for graphene and graphite in which the x-axis indicates the difference in wavelength between the incoming and outgoing photons. The incident photon can decrease or increase its energy by creating (Stokes process) or destroying (Anti-Stokes process) a phonon. Due to the conservation of energy and momentum, we have

$$\begin{aligned} E_s &= E_i \pm E_q \\ k_s &= k_i \pm q \end{aligned} \tag{2.1}$$

where E_i (k_i) is the energy (wavevector) of the incident photon, E_s (k_s) is the energy (wavevector) of the scattered photon and E_q (q) is the energy (wavevector) of the created or annihilated phonon where momentum and wavevector are related by $p = \hbar k$, $\hbar$ being the Planck's constant divided by 2π. The interaction between phonons and light is mediated by electrons, and the strength with which this interaction occurs depends on the polarizability of the material. At very specific energies, resonances can occur and the shape of the Raman peak can be described reasonably well as the response of a damped harmonic oscillator (corresponding to one lattice mode with wavevector q) with a characteristic frequency ω_q forced by an external field (light) of frequency ω and damping parameter Γ_q. Thus, the intensity of the peak is of the form

$$I(\omega) = \frac{I_0}{\pi\Gamma_q} \frac{1}{(\omega - \omega_q)^2 + \Gamma_q^2}. \tag{2.2}$$

The damping energy is related to the lifetime of the phonons. The energy-time uncertainty principle gives an uncertainty in the phonon energy given by $\Delta E \Delta t \approx \hbar$ from which we can relate the damping parameter with the inverse lifetime of a phonon. There are several reasons why phonons have a finite lifetime. On the one hand, the anharmonicity of the potential, which is responsible for thermal expansion and the finite thermal conductivity, causes phonon-phonon interaction. Additionally, phonons interact with electrons, which may cause the excitation of an electron from the valence band to the conduction band. Finally, impurities in the crystal may cause phonon-impurity scattering, and this will be the main topic of this thesis.

2.1.1 Quantum Description of the Raman Process

A realistic description of the Raman process requires us to describe the physics from a quantum-mechanical point of view. As mentioned before, the interaction between light and phonons is mediated by electrons and, therefore, a large number of different processes are possible. To keep track of all the relevant processes that may occur, Feynman diagrams, such as those shown in Fig. 2-2, are useful. Such diagrams simplify the interpretation of the Raman process. Each node on this diagram represents

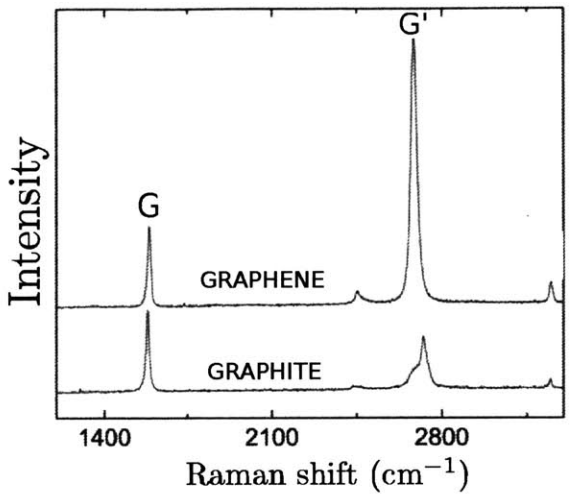

Figure 2-1: Typical Raman spectra of graphene. Typical features include the symmetry-allowed G-band and the G'-band. Other lower intensity features also are observed, but not discussed further in this thesis.

an interaction, which translates into matrix elements of the interaction between electrons, phonons and photons in the Raman calculation. A typical Raman intensity calculation involves calculating these matrix elements and obtaining expressions of the type

$$I \propto \left| \sum_{k,k'} \frac{\langle i|\mathcal{H}_{eR}(\omega_s)|k'\rangle\langle k'|\mathcal{H}_{e-ph}(q)|k\rangle\langle k|\mathcal{H}_{eR}(\omega_{\text{laser}})|i\rangle}{[E_{\text{laser}} - (E_k - E_i)][E_{\text{laser}} - \hbar\omega_q - (E_{k'} - E_i)]} \right|^2 \delta(E_{\text{laser}} - \hbar\omega_q - \hbar\omega_s) \quad (2.3)$$

where $|i\rangle(E_i)$ denotes the initial state (energy) of the system, ω_{laser} (E_{laser}) is the frequency (energy) of the incoming phonons (the source is a laser line), ω_s is the frecuency of the scattered photons, k (E_k) and k' ($E_{k'}$) represent intermediate electronic states (energies), and $\mathcal{H}_{eR}(\mathcal{H}_{e-ph})$ denotes the electron-photon (electron-phonon) interaction matrix. Higher order processes will include more nodes in the diagram, and will result in more complicated expressions than Eq. (2.3), but the idea is still the same. In this work we focus on the effect of the phonon lifetime on the Raman spectra, so it will not be necessary to evaluate expressions of the form of Eq. (2.3). A detailed description of the Raman calculation can be found in [1].

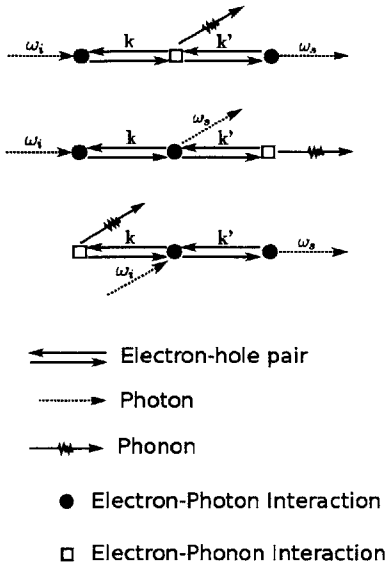

Figure 2-2: Examples of Feynman diagrams for scattering processes that contribute to Stokes Raman scattering. Here ω_i (ω_s) is the frequency of the incident (scattered) photon and k and k' are the corresponding wavectors of electron-hole states. Each node represents an interaction between an electron and a photon or between an electron and a phonon.

2.2 Isotope impurities

The ^{13}C isotope exists in natural carbon in a 1.1% abundance and the remaining 98.9% are ^{12}C. Because of the low concentration of ^{13}C, we can usually neglect this isotope effect for discussing the physical properties of graphene-related materials. However, if we consider, for example, the intrinsic spectral linewidth in Raman spectroscopy, the isotope effect might be essential as one of the important intrinsic scattering mechanisms. When we intentionally increase the ^{13}C isotope concentration in an sp^2 material, the resulting graphene-related material made of varying concentrations of ^{13}C has provided interesting information for gaining a better understanding of phonon related properties [48] as well as growth mechanisms [49, 50]. The advantage of the isotope enrichment technique is that only phonon frequencies or thermal properties can be modified without changing the electrical or chemical properties, so that we can distinguish effects due to the electron-phonon interaction from those associated with electronic or electron-electron interactions in making assignments for unassigned

optical spectral features [48, 51, 52]. In the case of crystal growth, if we substitute a ^{12}C atom in a gas source molecule by a ^{13}C atom, we can get information on how the carbon atoms from the gas molecule are used for the crystal growth of carbon nanotubes [49] and graphene [50].

Miyauchi *et al.* [48] made a 100% ^{13}C single wall carbon nanotube (SWNT) sample by chemical vapor deposition using ^{13}C ethanol. Comparing the Raman spectra of ^{13}C SWNTs and ^{12}C SWNTs, they assigned the phonon-assisted peaks in the photoluminescence spectra. Kalbac *et al.* [51] observed the Raman spectra of a special bilayer graphene sample on a substrate, in which the top (bottom) layer of the bilayer graphene consisted of pure ^{12}C (^{13}C) so that they could separately investigate the single layer components of bilayer graphene. Costa *et al.* [3] observed a frequency shift and broadening of the Raman G-band in single wall carbon nanotubes as a function of ^{13}C concentration, and they suggested that these effects were caused by phonon localization due to the elastic scattering of phonons by the ^{13}C atoms [3]. In addition, they studied the laser energy dependence of the G' and D bands for pure ^{12}C and pure ^{13}C samples. They found for each band that the slope of the curve, which is sensitive to the electronic structure, does not change with the isotope mass. This result serves as strong experimental evidence that isotope enrichment does not modify the electronic structure.

Many theoretical works are focused on thermal transport properties of isotope-enriched samples. Savić *et al.* [53] studied the phonon transport of isotope disordered SWNTs and boron nitride nanotubes in the presence of isotope disorder by an *ab initio* calculation. They calculated the reduction in thermal conductivity due to the impurities, and they concluded that the reduction is mostly due to diffusive scattering of phonons by the isotopes. More recently, Yamamoto *et al.* [54] extended the previously mentioned calculations to study phonon transmission fluctuations in carbon nanotubes, finding a universal behavior with respect to phonon transmission, tube chirality, and concentrations and masses of isotopes. In these two works [53, 54], the three transport regimes (ballistic, diffusive and localized) are observed, and localization lengths are calculated via atomistic Green's function formalisms, while local-

ization effects of the phonon wavefunction are not discussed. As pointed out by Savić *et al.*, localization effects are difficult to observe in thermal transport measurements because the thermal conductance is mostly dominated by the ballistic and diffusive contributions. The localization regime appears in the high-energy optical modes, and thus special experimental techniques capable of probing these high-energy modes are required to observe any localization effects.

We are here interested in optical phonon scattering and the localization effect in graphene which are the main topics of the present thesis. Phonon localization is another example of Anderson's localization theory [55, 56], which is applicable to several wave phenomena like light [57] or water waves [58], but has in the past been mostly associated with electronic transport in disordered crystals. When the phonon wavefunction is localized, the phonon mean free path λ_{ph} becomes finite and proportional to the square of the localization length λ .

When we discuss the electron-phonon interaction of graphene [59, 60], we generally treat the phonon wavefunction as delocalized in the crystal. However, in a naturally ocurring graphene sample, we know that 1.1% of the atoms are ^{13}C and thus phonons have a finite lifetime τ and a finite localization length λ due to the phonon scattering by ^{13}C, which is one of the main contributions to the natural linewidth γ of the Raman spectra. Further, we need theoretical understanding on how the localization length λ of the phonon is changed as a function of ^{13}C concentration so that we can explain the experimental observations of Costa *et al* [3].

In this work, we calculate the phonon wavefunction in a large unit cell, large enough so that the localization length λ is smaller than the size of this unit cell. When we add an impurity to a perfect crystal lattice, the translational symmetry is broken, and the wavevectors associated with the unit cell are no longer good quantum numbers. This means that phonons are scattered into other states, and some of the wave functions are localized in real space by mixing many q-states, where q is the phonon wavevector.

It should be mentioned that the anharmonicity of the vibration also produces phonon scattering. However, we do not include here this effect for simplicity. Since

the anharmonicity effect should be significant for large phonon amplitudes, this phenomenon is important only for high temperatures and can, in principle, be tuned in experiments.

Our objective in the present work is two-fold. On the one hand, we calculate the optical phonon lifetimes due to impurity scattering in order to have a value to compare with competing processes. The advantage of performing this estimation is that, assuming all scattering processes to be independent (Matthiessen's rule), our calculation of λ provides a way to directly compare the lifetimes of the different interactions which are important for phonon properties, such as the electron-phonon interaction and localization effects. Additionally, we calculate the localization length as a function of impurity density to study localization effects caused by isotope impurities. We focus particularly on the LO and iTO modes because of their importance in the Raman G-band.

2.3 Phonons

We solve the phonon lifetime and localization problem within the harmonic approximation in which up to 4-th nearest neighbor interactions are considered and use the force constants of Jishi *et al* [4]. The unit cell and the BZ of graphene are shown in Fig. 2-3. The effect of adding a ^{13}C isotope impurity to the lattice will not modify the force constant parameters, as the extra neutron in each nucleus will not modify the chemistry of the bonding. However, the isotope impurity will affect the dynamics due to the increased mass of the ion which is incorporated into the perturbed Hamiltonian. In 2.3.1 we briefly describe the solution to the unperturbed problem, in which we obtain expressions that will be useful for calculating phonon lifetimes, and in 2.3.2 we introduce perturbations in describing the model we used for the estimation of phonon lifetimes.

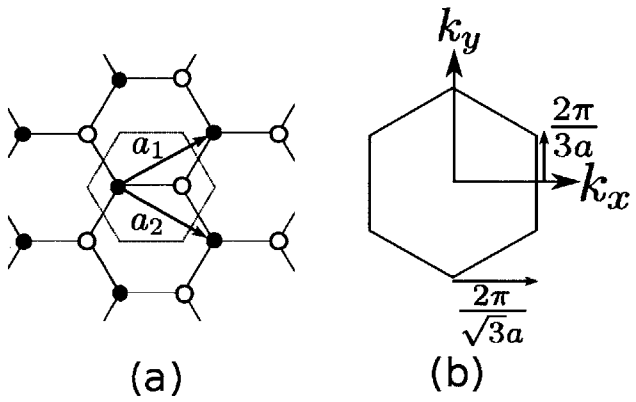

Figure 2-3: (a) Unit cell of graphene and the translation unit vectors a_1 and a_2. (b) The BZ of graphene. Here a is the lattice constant of graphene (0.246 nm). From Ref. [2].

2.3.1 Unperturbed Hamiltonian

The unperturbed Hamiltonian of phonons, within the harmonic approximation, is given by

$$H = \sum_{i,\nu} \frac{\mathbf{p}_i^\nu \cdot \mathbf{p}_i^\nu}{2m_\nu} + \sum_{i,j,\nu,\nu'} \frac{\mathbf{u}_i^\nu V_{ij}^{\nu\nu'} \mathbf{u}_j^{\nu'}}{2}, \tag{2.4}$$

where the subscript i labels the unit cell in the supercell and ν labels the atom within the unit cell (i.e., $i = 1, 2, ..., N$, and $\nu = 1, 2$ which corresponds to the graphene sublattice A or B, respectively) and $\mathbf{u}_i^\nu$ and $\mathbf{p}_i^\nu$ are the amplitude and momentum of vibrations at the (i,ν)-th atom, respectively. The term $V_{ij}^{\nu\nu'}$ is the interaction potential between the atoms at (i, ν) and (j, ν'), and m_ν is the mass of the atom at site ν within the unit cell. $\mathbf{u}_i^\nu$ and $\mathbf{p}_i^\nu$ satisfy the commutation relation

$$[u_{il}^\nu, p_{jl'}^{\nu'}] = i\hbar\delta_{ij}\delta_{\nu\nu'}\delta_{ll'}, \tag{2.5}$$

where $l, l' = x, y, z$. $\mathbf{u}_i^\nu$ and $\mathbf{p}_i^\nu$ can be expressed by a Fourier transformation for wavevectors q within the BZ

$$\mathbf{u}_i^\nu = \sum_q \frac{e^{iq\cdot r_i^\nu}}{\sqrt{N}} \mathbf{u}_q^\nu, \tag{2.6}$$

and

$$\mathbf{p}_i^\nu = \sum_q \frac{e^{-iq\cdot r_i^\nu}}{\sqrt{N}} \mathbf{p}_q^\nu, \tag{2.7}$$

where r_i^ν is the equilibrium position of atom (i, ν). Then Eq. (2.4) can be expressed in terms of q rather than i, j

$$H = \sum_{q,\nu} \frac{\mathbf{p}_q^\nu \cdot \mathbf{p}_q^{\nu\dagger}}{2m_\nu} + \sum_{q,\nu,\nu'} \frac{\mathbf{u}_q^{\nu\dagger} V_q^{\nu\nu'} \mathbf{u}_q^{\nu'}}{2}, \tag{2.8}$$

where $V_q^{\nu\nu'} = \sum_j V_{ij}^{\nu\nu'} e^{iq\cdot(r_j^{\nu'} - r_i^{\nu'})}$. We diagonalize the Fourier transform of the interaction potential Φ_q according to

$$\sum_{\nu'} \frac{V_q^{\nu\nu'}}{\sqrt{m_\nu m_{\nu'}}} \mathbf{e}_{q,n}^{\nu'} = \omega_{qn}^2 \mathbf{e}_{qn}^\nu, \tag{2.9}$$

where ω_{qn} ($\mathbf{e}_{qn}$) is the eigenvalue (eigenvector) of the n-th normal phonon mode for wavevector q. The eigenvectors $\mathbf{e}_{qn}$ satisfy the normalization condition $\sum_\nu \mathbf{e}_{qn}^{\nu *} \cdot \mathbf{e}_{qn'}^\nu = \delta_{nn'}$. Further, we define the displacement X_{qn} of the n-th normal mode with wavevector q by

$$X_{qn} = \sum_\nu \sqrt{m_\nu} \mathbf{e}_{qn}^{\nu *} \cdot \mathbf{u}_q^\nu, \tag{2.10}$$

and similarly for the momentum

$$P_{qn} = \sum_\nu \frac{1}{\sqrt{m_\nu}} \mathbf{e}_{qn}^\nu \cdot \mathbf{p}_q^\nu. \tag{2.11}$$

The Hamiltonian of Eq. (2.8) is thus simplified to

$$H = \sum_{q,n} \frac{P_{qn} P_{qn}^\dagger}{2} + \frac{\omega_{qn}^2 X_{qn}^\dagger X_{qn}}{2}, \tag{2.12}$$

where $[X_{qn}, P_{q'n'}] = i\hbar\delta_{qq'}\delta_{nn'}$. Finally we define the annihilation and creation operators, respectively, as

$$a_{qn} = \sqrt{\frac{\omega_{qn}}{2\hbar}}(X_{qn} + iP^{\dagger}_{qn}/\omega_{qn}), \tag{2.13}$$

and

$$a^{\dagger}_{qn} = \sqrt{\frac{\omega_{qn}}{2\hbar}}(X^{\dagger}_{qn} - iP_{qn}/\omega_{qn}), \tag{2.14}$$

which satisfy $[a_{qn}, a^{\dagger}_{q'n'}] = \delta_{qq'}\delta_{nn'}$. The Hamiltonian now becomes

$$H = \sum_{qn} \hbar\omega_{qn}(a^{\dagger}_{qn}a_{qn} + \frac{1}{2}). \tag{2.15}$$

2.3.2 Estimation of the Phonon lifetime

There are two ways to calculate the phonon lifetime for each phonon mode. In the first approach, we can use the eigenstates and eigenvalues found for a large graphene supercell and use these values to determine the T-matrix [61]. In the second approach we can treat the change in the mass matrix as a perturbation and find the phonon lifetime using perturbation theory. We use the second approach to gain better physical insight and to obtain explicit analytic expressions.

If we add ^{13}C isotope impurities into the lattice, we can consider the Hamiltonian in Eq. (2.4) in which we set the mass m_ν equal to the average mass $\bar{m} = \sum_{i,\nu} m_{i,\nu}/2N$. Then, the perturbation to the Hamiltonian ΔH is due to the kinetic term (expressed in terms of velocities) and given by

$$\Delta H = \sum_{j\nu'} \frac{f^{\nu'}_j}{2}\bar{m}\dot{\mathbf{u}}^{\nu'}_j \cdot \dot{\mathbf{u}}^{\nu'}_j, \tag{2.16}$$

where $f^{\nu'}_j = (m^{\nu'}_j - \bar{m})/\bar{m}$. We can express Eq. (2.6) in terms of creation and annihilation operators $a^{\dagger}_{qn}$ and a_{qn} using Eqs. (2.13) and (2.14)

$$\mathbf{u}^{\nu'}_j = \sum_{qn} \sqrt{\frac{\hbar}{2N\bar{m}\omega_{qn}}} e^{iq\cdot r^{\nu'}_j}(a_{qn} + a^{\dagger}_{-qn})\mathbf{e}^{\nu'}_{qn}, \tag{2.17}$$

and then replace Eq. (2.17) in Eq. (2.16) to obtain

$$\Delta H = \sum_{qq'nn'} h_{qq'}^{nn'} (a_{qn} a_{-q'n'}^{\dagger} + a_{-qn}^{\dagger} a_{q'n'}), \tag{2.18}$$

where we dropped the terms involving the product of two creation (annihilation) operators as they do not conserve energy. These two terms that were dropped are going to be relevant beyond second order perturbation theory. The amplitude for scattering a phonon from q to q', denoted by $h_{qq'}^{nn'}$, is given by

$$h_{qq'}^{nn'} = \frac{\hbar R(q,q')}{4N} \sqrt{\omega_{qn}\omega_{q'n'}} \sum_{\nu'} \mathbf{e}_{qn}^{\nu'} \cdot \mathbf{e}_{q'n'}^{\nu'}, \tag{2.19}$$

where we defined $R(q,q')$ as

$$R(q,q') = \sum_j f_j^{\nu'} e^{i(q+q')\cdot r_j^{\nu'}}. \tag{2.20}$$

We can use the Fermi golden rule to determine the transition rates $P_{i\to f}$ for phonon scattering from the initial state (i) to final state (f)

$$P_{i\to f} = \frac{2\pi}{\hbar} |\langle f|\Delta H|i\rangle|^2 \delta(E_f - E_i), \tag{2.21}$$

within second order perturbation theory. The transition probability for scattering from state (q,n) to (q',n') is given by

$$P_{qq'}^{nn'} = \frac{2\pi}{\hbar} N_{qn}(N_{q'n'}+1)|h_{qq'}^{nn'}|^2 \delta(\hbar\omega_{qn} - \hbar\omega_{q'n'}), \tag{2.22}$$

where N_{qn} ($N_{q'n'}$) is the number of phonons in state (q,n) ((q',n')), and the lifetime of the phonon mode (q,n) is then given by

$$\tau_{qn}^{-1} = \frac{\pi}{2N^2} \sum_{q'n'} |R(q,q')|^2 \omega_{qn}\omega_{q'n'} (\mathbf{e}_{qn}^{*} \cdot \mathbf{e}_{q'n'})^2 \delta(\omega_{qn} - \omega_{q'n'}). \tag{2.23}$$

Because we assume that the impurities are randomly distributed, we can use the random phase approximation to evaluate $|R(q,q')|^2$. If we take an ensemble average

of $|R(q,q')|^2$ over different realizations of the isotopically doped samples

$$\langle |R(q,q')|^2 \rangle = \left\langle \sum_{j,l} f_j^{\nu'} f_l^{\nu'} e^{i(q+q')\cdot(r_j^{\nu'} - r_l^{\nu'})} \right\rangle, \tag{2.24}$$

we obtain

$$\langle |R(q,q)|^2 \rangle = \sum_j f_j^{\nu'} f_j^{\nu'} = \frac{N\Delta m^2 \rho(1-\rho)}{(m_0 + \rho\Delta m)^2}, \tag{2.25}$$

where ρ is the number density of ^{13}C ($0 \leq \rho \leq 1$), m_0 is the mass of ^{13}C and Δm is the mass difference between ^{12}C and ^{13}C isotopes. We discussed previously that our unperturbed Hamiltonian of Eq. (2.4) is the one corresponding to the average mass $\bar{m}$ so that the frequency spectrum is equivalent to the one corresponding to pure ^{12}C but scaled as $\propto (\bar{m})^{-1/2}$ in the case of general ρ. Thus, if we rescale frequencies as $\omega = \omega^0\sqrt{\bar{m}/m_0}$, where m_0 is the mass of ^{12}C, we can factorize the density ρ and isotope mass dependence $(m_0 + \Delta m)$ from the summation in Eq. (2.23), yielding

$$\tau_{qn}^{-1} = \frac{\pi f(\rho)}{2N} \sum_{q'n'} \omega_{qn}^0 \omega_{q'n'}^0 (\mathbf{e}_{qn}^* \cdot \mathbf{e}_{q'n'})^2 \delta(\omega_{qn}^0 - \omega_{q'n'}^0), \tag{2.26}$$

where the frequencies ω_{qn}^0 correspond to the n-th phonon mode frequency at q of ^{12}C. The function $f(\rho)$ contains all the information about isotope mass and density;

$$f(\rho) = \frac{\Delta m^2 \rho(1-\rho)}{(m_0 + \rho\Delta m)^2} \sqrt{\frac{m_0}{m_0 + \rho\Delta m}}. \tag{2.27}$$

The function $f(\rho)$ is plotted vs. isotope density ρ in Fig. 2-4 for the cases of ^{13}C and ^{14}C. Here we see that the effect of using ^{14}C instead of ^{13}C in doping ^{12}C produces a reduction of the lifetime by a factor of approximately 4. However, ^{14}C is an unstable isotope, while ^{13}C is stable and is found in naturally occurring materials. Thus we focus on ^{13}C for the rest of the thesis. Nevertheless, we keep in mind that using ^{14}C just changes the prefactor of Eq. (2.26) as plotted in Fig. 2-4. In addition, we can transform Eq. (2.23) into an integral over the BZ, yielding

$$\tau_{qn}^{-1} = \frac{f(\rho) S}{8\pi} \sum_{n'} \int d^2q' \omega_{qn}^0 \omega_{q'n'}^0 (\mathbf{e}_{qn}^* \cdot \mathbf{e}_{q'n'})^2 \delta(\omega_{qn}^0 - \omega_{q'n'}^0), \tag{2.28}$$

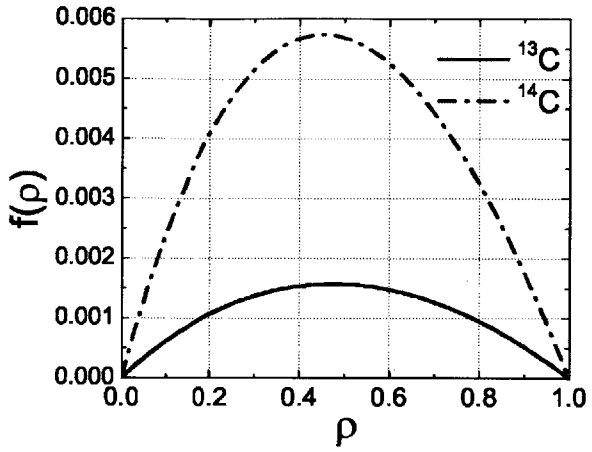

Figure 2-4: Isotopic density dependence of the lifetime given by the function $f(\rho)$ as defined in Eq. (2.27). From Ref. [2].

where S is the area of the unit cell. Here we emphasize again that the term inside the summation of Eq. (2.28) has no dependence on impurity density or isotope mass, so that the integration of Eq. (2.28) can be done using pure ^{12}C eigenstates and eigenvalues, independent of the particular isotopically doped sample we are considering. Therefore, we can express Eq. (2.28) as

$$\tau_{qn}^{-1}(\rho) = f(\rho) I_{qn}, \tag{2.29}$$

where the function $f(\rho)$ contains the density ρ dependence of the lifetime, while I_{qn} contains the wavevector (and frequency) dependence and gives the correct units of s^{-1}. The value of I_{qn} is increased as we go to modes with higher frequencies and in points of the BZ with a high density of states. In the next sections we will drop the superscripts 0 in Eq. (2.28) but taking into account that we are referring to the eigenstates and eigenvalues of a pure sample containing only ^{12}C atoms. Eq. (2.29) is the result of using second order perturbation theory and the random phase approximation. Inclusion of higher order terms in the perturbation expansion will result in a more complicated expression of the phonon lifetime in Eq. (2.29) in which the ρ density dependence can no longer be factorized.

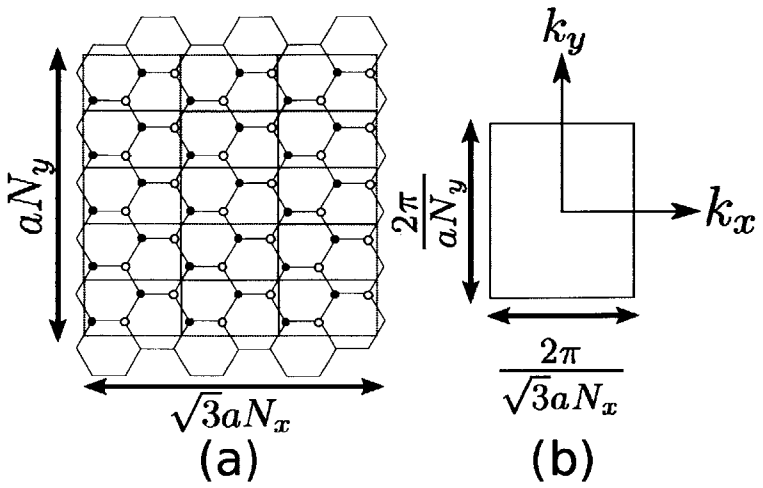

Figure 2-5: (a) An example of a supercell, with N=30 unit cells and 60 carbon atoms. Here N_x and N_y label the number of unit cells in the x and y directions, respectively. (b) The BZ of this supercell. From Ref. [2].

2.3.3 Localized states

To estimate the localization length λ of the localized states, we numerically solve the Hamiltonian of a supercell containing N unit cells of graphene. Even though this approach may become time consuming for unit cells large enough to do quantitative calculations, the advantage of numerically calculating the eigenstates and eigenvalues (as opposed to using perturbation theory) is that we can obtain additional information about the eigenstates that would be difficult to calculate otherwise. An example of the type of supercell consisting of $2N$ atoms that we used in our calculations is shown in Fig. 2-5. Here we introduced periodic boundary conditions for the supercell.

Because of the breaking of the translational symmetry by the introduction of ^{13}C impurity atoms, we change the labels from $\mathbf{u}_i^\nu$, with $i = 1, 2, ..., N$ and $\nu = 1, 2$, to $\mathbf{u}^\mu$, with $\mu = 1, 2, ..., 2N$. Therefore, the displacements $\mathbf{u}^\mu$ in the supercell have $6N$ components. The diagonalization of this problem is analogous to the case of the unperturbed Hamiltonian, but in this case we diagonalize the large $6N \times 6N$ (real) matrix $V^{\nu\nu'}$ according to

$$\sum_{\mu'} \frac{V^{\mu\mu'}}{\sqrt{m_\mu m_{\mu'}}} \mathbf{e}_j^{\mu'} = \omega_j^2 \mathbf{e}_j^\mu, (\mu = 1, ..., 2N; j = 1, ..., 6N), \tag{2.30}$$

in which ω_j ($\mathbf{e}_j^\mu$) is the eigenvalue (eigenvector) of the j-th normal mode. The orthonormal condition on the eigenvectors $\mathbf{e}_j^\mu$ is given by

$$\sum_{\mu=1}^{2N} \mathbf{e}_j^\mu \cdot \mathbf{e}_{j'}^\mu = \delta_{jj'}. \tag{2.31}$$

If we have extended states, on average $|\mathbf{e}_j^\mu| \approx 1/\sqrt{N}$. On the other hand, for a highly localized state we have $|\mathbf{e}_j^\mu| \approx 1$ for only a few atoms and $|\mathbf{e}_j^\mu| \approx 0$ for the rest. Therefore, we can distinguish localized states from non-localized states by defining the second moment of the displacement field A_j (also known as the inverse participation number [62]) as

$$A_j = \sum_\nu (\mathbf{e}_j^\nu \cdot \mathbf{e}_j^\nu)^2. \tag{2.32}$$

Most of the eigenstates will be extended states, in which case $A_j \approx 1/N$, while for localized states A_j is much larger and $A_j \approx 1$.

At the same time, the function A_j is also useful to estimate the localization length λ_j of the eigenstates j, since λ_j and A_j are related by $\lambda_j \propto A_j^{-1/2}$ [56]. As we know, for the ^{13}C concentration $\rho = 0$, all states are extended states. We can then estimate the localization length of state j by

$$\frac{\lambda_j}{\lambda_0} = \left(\frac{\bar{A}_0}{A_j}\right)^{1/2}, \tag{2.33}$$

where λ_0 is the size of the supercell and $\bar{A}_0$ is the average value of A_j for the special case of a pristine graphene sample with only ^{12}C atoms.

Chapter 3

RESULTS

3.1 Phonon lifetime

We calculated numerically the phonon lifetime for the elastic scattering process using Eq. (2.28). Even though we do not intend here to discuss acoustic phonon modes, we note that an analytical expression for the lifetime of the acoustic phonon modes can be obtained by similar means and can be found in the literature in relation to discussions of heat transfer [63]. This will be useful to obtain an idea about the order of magnitude of the optical phonon scattering process, but we also calculate numerically the values of τ_{qn}^{-1} from Eq. (2.28) for all phonon modes. Due to our special interest in the optical modes, we discuss these modes in more detail. Then we can compare the contribution to phonon scattering coming from the presence of isotopic impurities with competing processes contributing to τ_{qn}^{-1}.

3.1.1 Low energy acoustic phonon modes

For the case of low energy acoustic phonon modes in graphene, we have linear dispersion relations for the LA and iTA modes near the Γ-point, and a quadratic relation for the oTA mode. The integration of Eq. (2.28) over reciprocal space can be done analytically for the three acoustic modes. Because of the dot product term in Eq. (2.28), we have a decoupling in the expression of the in-plane and out-of-plane phonon modes.

For the in-plane modes we use $\omega_{q'n'} \approx c_{n'}q'$ in Eq. (2.28), where $c_{n'}$ is the velocity of the phonon mode. We can define further an average value over the BZ for the dot product of the polarization for the in-plane modes $p_{\text{in}} = \langle(\mathbf{e}^*_{qn} \cdot \mathbf{e}_{q'n'})^2\rangle$. The exact values for this polarization term in the case of graphene can be found in the paper by Lindsay *et al* [64]. Substituting p_{in} into Eq. (2.28) and solving the indicated integral we obtain

$$\tau_{qn}^{-1} = \frac{f(\rho)Sp_{\text{in}}}{4}\left(\sum_{n'} c_{n'}^{-2}\right)\omega_{qn}^3 = \frac{f(\rho)Sp_{\text{in}}}{2\bar{c}^2}\omega_{qn}^3 \tag{3.1}$$

where S is the area of the unit cell. Similarly, for the out-of-plane phonon modes using $\omega_{q'} = bq'^2$, and $p_{\text{out}} = \langle(\mathbf{e}^*_{qn} \cdot \mathbf{e}_{q',n'})^2\rangle$ for n =out-of-plane, we obtain for the oTA mode

$$\tau_{qn}^{-1} = \frac{f(\rho)Sp_{\text{out}}}{8b}\omega_{qn}^2. \tag{3.2}$$

The order of magnitude of the phonon lifetime of the optical in-plane modes (LA and iTA) due to isotopic impurities can be estimated by evaluating Eq. (3.1) at the BZ boundaries and using $S = 0.052$ nm^2, $p_{\text{in}} \approx 0.5$, $\bar{c} \approx 20$ km/s, $\hbar\omega_{qn} \approx 0.15$ eV (ω_{qn} at $q \approx \pi/a$) and evaluating $f(\rho)$ at the desired ^{13}C density. Therefore, the order of magnitude of the lifetime of an in-plane optical phonon mode for the natural ^{13}C isotopic density ($\rho = 0.011$) is $\tau \sim 30$ ps, and for a ^{13}C concentration of $\rho = 0.5$, we obtain a much shorter lifetime of $\tau \sim 1$ ps.

3.1.2 General Phonon Lifetime

For the general case of wave vector q and phonon mode n, we do a numerical integration of Eq. (2.28) over the BZ. The value of $(\tau f)^{-1}$ is plotted as a function of q in the BZ and for all phonon modes in Fig. 3-1. As discussed in connection with Eq. (2.29), the value of $(\tau f)^{-1}$ is independent of isotope density or isotope mass, and to obtain a numerical value for the phonon lifetime τ we must first calculate the value of $f(\rho)$ of Eq. (2.27) from Fig. 2-4 depending on the particular values of ^{13}C concentrations in the sample. As expected, optical phonon modes are sensitively affected by the isotope impurities, while acoustic modes close to the Γ-point are less affected. For the acoustic modes, and close to the Γ-point, we observe the power law behavior

obtained in the previous section, i.e., $(\tau f)^{-1} \propto \omega^3 \propto q^3$ for the in-plane modes, and $(\tau f)^{-1} \propto \omega^2 \propto q^4$ for the out-of-plane modes. There is also a large difference in the lifetime scale between in-plane and out-of-plane phonon modes due to the large difference in the stiffness of the relevant modes in graphene.

We now use the calculated values of the phonon lifetime for the optical modes at the Γ-point to make comparisons with previously calculated values of the electron-phonon coupling interaction in graphene. From Fig. 3-1 we obtain that at the Γ-point for the in-plane optical modes, $(\tau f)^{-1} \approx 0.8$ fs^{-1} and from Fig. 2-4, we obtain $f(0.5) = 1.5 \times 10^{-3}$ and $f(0.011) = 7.5 \times 10^{-5}$. Then, the value of the phonon lifetime due to ^{13}C impurities (no other lifetime limiting effects included) is $\tau_{\text{ph}-\text{imp}} \approx 0.83$ ps for an isotopic atomic density of $\rho = 0.5$, and a value $\tau_{\text{ph}-\text{imp}} \approx 16.7$ ps for naturally occurring carbon. Previously calculated results for the electron-phonon coupling at the Γ-point of the optical modes [65, 66] are on the order $\tau_{\text{e}-\text{ph}} \approx 0.6$ ps. Thus, it is expected that for high concentrations of isotope impurities, the scattering rates for the isotopic impurity can become as large as that for the electron-phonon interaction. However, for concentrations lower than $\rho = 0.1$, the isotope effect makes only a minor contribution to the phonon lifetime when compared to the electron-phonon interaction for optical phonon modes.

Using the experimental values in Costa *et al.* [3] and assuming the Matthiessen rule holds for the two scattering mechanisms ($\tau_{\text{ph}}^{-1} = \tau_{\text{ph}-\text{imp}}^{-1} + \tau_{\text{e}-\text{ph}}^{-1}$), we can estimate the contribution of the isotope impurities to the spectral width of the G-band γ_{G}. We plot in Fig. 3-2 the experimental values of $\gamma_{\text{G}}^{\text{exp}}$ (full-width at half maximum (FWHM)) and, taking into account that the spectral width γ is related to the lifetime τ as $\gamma \propto \tau^{-1}$, we fit these values as

$$\gamma_{\text{G}} = \gamma_{\text{e}-\text{ph}}^{\text{exp}} + \gamma_{\text{ph}-\text{imp}}^{\text{exp}} \frac{f(\rho)}{f(0.5)}, \tag{3.3}$$

where $f(\rho)$ is defined in Eq. (2.27), and where we assume that the electron-phonon coupling is the main competing process. The value $\gamma_{\text{ph}-\text{imp}}^{\text{exp}}$ obtained from the fitting as defined in Eq. (3.3) corresponds to the linewidth at a ^{13}C concentration of $\rho = 0.5$.

The values obtained from the fitting are $\gamma_{e-ph}^{exp} = 11.2 \pm 0.4$ cm^{-1} and $\gamma_{ph-imp}^{exp} = 5.2 \pm 0.4$ cm^{-1} and the curve for $\gamma_G(\rho)$ is plotted with dashed lines in Fig. 3-2. We see that the experimental data are well described by the dashed curve for our model. The in-plane phonon optical modes at the Γ-point make the main contribution to the G-band in Raman spectroscopy. If we consider our calculated value of the phonon lifetimes at the Γ-point of the in-plane optical modes ($\tau_{ph-imp} \approx 0.83$ ps), and using the uncertainty principle, we obtain $\gamma_{ph-imp} \approx \hbar/\tau_{ph-imp} \approx 6.0$ cm^{-1}. This result is in good agreement with the experimental result of 5.2 cm^{-1}.

Considering that isotopic defects do not interact directly with electrons, we expect our results to extend to other Raman features. In particular, isotope impurities alone cannot account for the presence of the D-band because of the null matrix elements for elastic scattering of the electrons by the isotopic defects. The D-band, if present, should originate from other types of defects and the main contribution of ^{13}C atoms would be to shift the D-band frequency due to the mass effect and change the spectral width due to the reduced phonon lifetime.

3.2 Phonon Localization

To find the phonon localization length we first compute $A_j = \sum_\mu (\mathbf{e}_j^\mu \cdot \mathbf{e}_j^\mu)^2$ (Eq. (2.32)) for random impurities at different impurity concentrations ρ in a supercell. In Chapter 2 we discussed the case where if the phonon wavefunction is highly localized, A_j is close to 1, while if it is delocalized, A_j scales as $1/N$. For our calculations we used a supercell containing $N = 2700$ unit cells ($\lambda_0 \approx$13 nm) which, for natural carbon, contains 59 impurity atoms. In Fig. 3-3 we plot the phonon dispersion of graphene as well as the localization length as a function of energy for the different eigenstates and for an impurity density of ρ=0.1 and ρ=0.2. The localization length was normalized by $\lambda_0 = 13$ nm as described in section 2.3.3. Here it is shown that most states will be extended ($\lambda/\lambda_0 \approx 1$) within the size of our supercell, but a few states are localized. These localized states do not occur at random energies but rather occur preferentially at high phonon energies and in regions with flat phonon

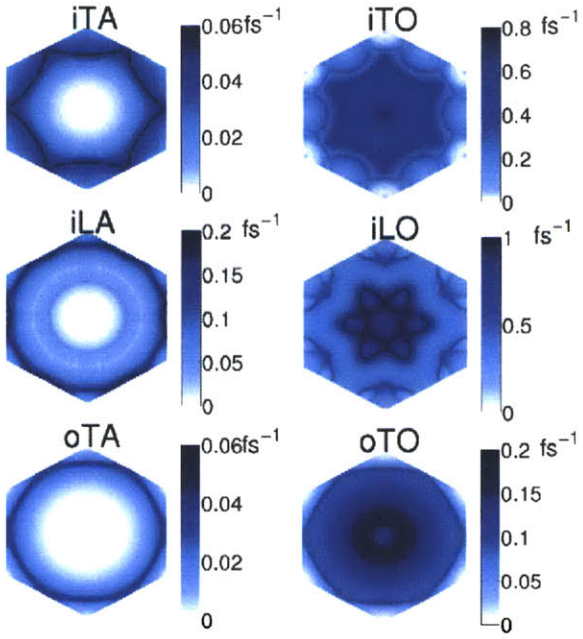

Figure 3-1: Plot of $I_{qn} = (\tau f)^{-1}$ for the different phonon modes and wavevectors in the two dimensional BZ as defined in Eq. (2.29), where $f(\rho)$ is defined in Eq. (2.27) and plotted in Fig. 2-4. Intensity scales are plotted beside each mode map. In-plane optical phonon modes (iTO and iLO) have a significantly lower lifetime than the other modes. From Ref. [2].

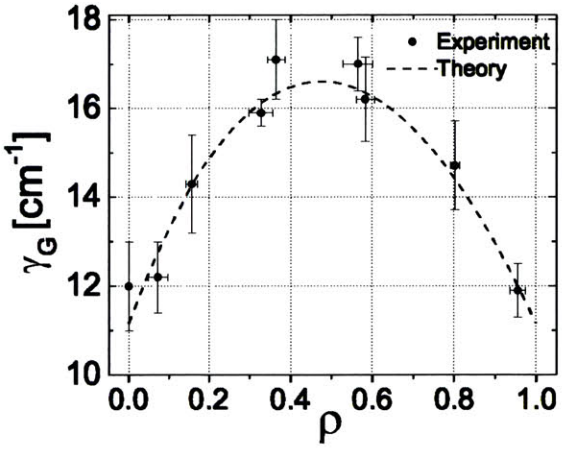

Figure 3-2: The points are the experimental values for the spectral width γ_G (FWHM) of the G-band obtained by Costa *et al.* [3] and the dashed curve is γ_G obtained by fitting Eq. (3.3) with the values of $\gamma^{\rm exp}_{\rm e-ph} = 11.2 \pm 0.4$ cm^{-1} and $\gamma^{\rm exp}_{\rm ph-imp} = 5.2 \pm 0.4$ cm^{-1}. From Ref. [2].

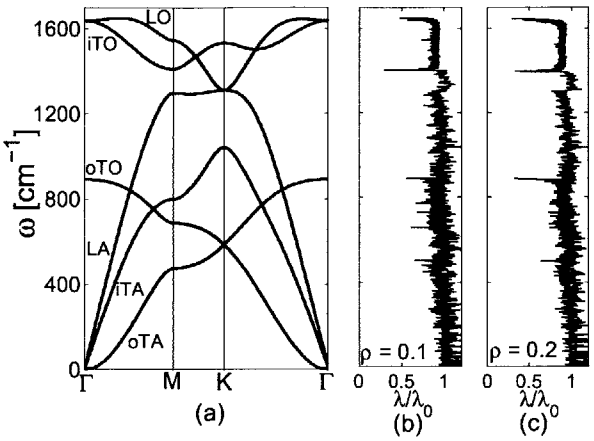

Figure 3-3: (a) Phonon dispersion for monolayer graphene [4]. (b,c) Normalized localization length λ/λ_0 (λ_0 is the size of super cell) as a function of the phonon frequency for the atomic isotope impurity densities of (b) ρ=0.1 and (c) ρ=0.2 (surface densities of 3.8 and 7.6 nm^{-2}, respectively). From Ref. [2].

dispersion (near the M or Γ-points). For high frequencies, and in regions with flat phonon dispersions, backscattering effects become increasingly important and thus localized wavefunctions are observed. It is in these regions of the spectrum where the localized regime is established when considering phonon transport, as discussed in Savić *et al* [53]. Here we calculate directly the localization length of the wavefunction using the inverse participation number A_j. Calculated characteristic lengths of a few nanometers for the localization length λ are comparable to those found using a different approach in Savić *et al.* [53] and Yamamoto *et al.* [54] in the high energy spectrum (in the proximity of 1600 cm^{-1} where the Raman G-band is located).

In the case of 1-D crystals, it can be shown that all states become localized due to random impurities [56], and in the case of 2-D crystals, a similar behaviour is expected as in the 1-D case. In the case of 3-D crystals, however, a transition from extended to localized states is expected as the energy is moved towards the band edge energies. This shows that localization phenomena is strongly dependent on dimensionality and therefore, careful attention should be paid when comparing localization-related results for nanotubes and graphene. Considering that the localized states under consideration have localization lengths on the order of a typical nanotube diameter, the comparison

is valid in this case but is no longer valid when considering lower frequency phonons with localization lengths on the micrometer scale. In addition, the parameter space when studying localization phenomena in carbon nanotubes is very rich because of the tube diameter and chirality dependence which is not present in graphene.

In this work we mainly focus on the Γ-point of the in-plane optical modes (LO and iTO branches) due to the dominant effect of these modes on the large G-band feature of the Raman spectra. Thus, the present size of the supercell is sufficient for our purposes of examining localization effects due to ^{13}C impurities. We also plot in Fig. 3-3 the calculated values for the out-of-plane phonon modes, where localization effects are also visible in Figs. 3-3 (b) and 3-3 (c) ($\omega \approx 900$ cm^{-1}). Infrared measurements of these modes may provide further information on localization phenomena in this range of frequencies. Even though a softening of the out-of-plane force constants may provide an enhanced effect, it is not clear if this effect will be dominant in an experiment because there will also be an increase of stiffness when considering the interaction of graphene with the substrate (increase of the out-of-plane force constants) or curvature effects if the experiments are done with carbon nanotubes.

In Fig. 3-4 (a) we plot the average localization length λ for optical modes in a phonon frequency interval corresponding to the Γ-point of the in-plane optical modes ($\omega \approx 1600$ cm^{-1}) as a function of ^{13}C isotope concentration ρ. From the calculations, a typical localization length is on the order of $\lambda \approx 3$ nm. Examples of the average displacement $|u|$ of the atoms with respect to their equilibrium position as a function of position (projected on the x-axis) for localized states are shown in Figs. 3-4 (b) and (c) for two samples with $\rho = 0.2$ and $\rho = 0.4$, respectively. Many factors contribute to having an asymmetric curve after averaging over many eigenstates. On the one hand, the effect of increasing the mass of a small number of atoms in the lattice (by adding ^{13}C impurities to a ^{12}C lattice) is not the same as decreasing the mass of a small number of atoms in the lattice (by adding ^{12}C impurities to a ^{13}C lattice). As discussed before, the localization length is calculated from the inverse participation number A_j since $\lambda_j \propto A_j^{-1/2}$, and A_j is calculated using the amplitudes of the atoms in the eigenstate j. When we decrease the mass of a small number of atoms, the

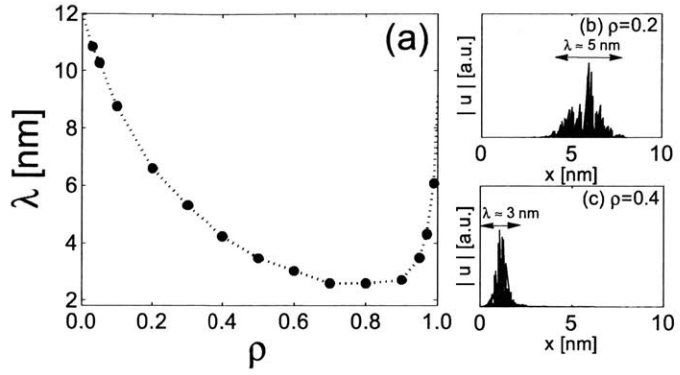

Figure 3-4: (a) Localization length λ at the Γ-point of the optical phonon modes as a function of ^{13}C atomic density ρ. (b,c) Displacement (in arbitrary units) of two different localized eigenstates as a function of position (projected on the x-axis) for an in-plane optical mode at the Γ-point and corresponding to ^{13}C concentrations of (b) $\rho = 0.2$ and (c) $\rho = 0.4$. From Ref. [2].

amplitude of these atoms with decreased mass within some (optical) eigenstate will be larger than the corresponding amplitude of the eigenstate in the pristine samples, and the opposite happens when increasing the mass of a small number of atoms. Therefore, even though in both cases the participation number will be larger than the one corresponding to the pristine sample eigenstates, the effect of isotope doping will be more abrupt in the first (decreasing mass) case. In addition, as the frequency of an oscillator scales with mass m as $\propto m^{-1/2}$, when we change the ^{13}C density of the sample, there are considerable changes in the density of states and therefore, when averaging over a frequency window, the comparison of localization lengths λ at different densities ρ is not straight-forward. The physics behind the localization of the eigenstates is related to the formation of islands of lower mass that vibrate at a different frequency from the rest of the lattice. At a 3 nm length scale, for example, around 100 atoms are vibrating in the localized mode and this regime corresponds to the case of weak localization [67].

Chapter 4

CONCLUSIONS

In this thesis we review the most commonly known types of defects in nano-carbon systems and emphasize the importance of understanding their effect on the properties of the materials. We argued that even though 'perfect' graphene has remarkable properties, actual graphene samples contain impurities. Even though impurities can degrade some of the properties of a perfectly crystalline system, in some cases impurities can also be beneficial. Our main focus in this work is to gain an understanding how defects change the properties of graphene. The final goal is understanding the limitations of devices as well as exploiting defect physics for technological purposes.

In the present work we studied the effects of ^{13}C isotope doping on the optical phonon modes of graphene. Here we calculated the values of the phonon lifetimes due to isotope impurity scattering for all values of ^{13}C densities and for all wavevectors within second order perturbation theory. These values are important for understanding the details of the Raman spectra of graphene and, in particular, the spectral width of the Raman features. Phonon lifetimes of optical phonon modes are considerably smaller (0.8 ps) than the corresponding lifetimes of the acoustic modes (which scale as a power law of the frequencies). We found that for natural concentrations of ^{13}C, the contribution of isotopic scattering of optical modes is negligible when compared to the electron-phonon interaction. Nevertheless, for atomic concentrations as high as $\rho = 0.5$, both contributions become comparable. Our results were compared with recent experimental results of ^{13}C Raman spectroscopy of nanotubes [3] and good

agreement was found for both the density dependence of the lifetime as well as in the calculated spectral width of the G-band. We predicted that the reduction of phonon lifetimes by changing ^{13}C isotopes to ^{14}C would be approximately fourfold.

The localization of optical phonons due to isotope impurities in graphene is calculated by the supercell method. Due to phonon scattering by ^{13}C isotopes, some graphene wavefunctions become localized in real space. Localized states appear predominantly in the high-energy optical phonon modes and in regions of flat phonon dispersion, where backscattering effects become increasingly important. A typical localization length is on the order of 3 nm for optical phonon modes at high concentrations of ^{13}C (in the range of number densities $\rho = 0.2 - 0.8$). Even though we focused attention mostly on in-plane optical modes, out-of-plane phonon modes may also provide a way to measure phonon localization effects and can be studied experimentally by infrared measurements. Even though these modes may also show pronounced localization effects due to reduced out-of-plane force constants, the coupling of graphene with the substrate (or curvature effects when considering nanotubes) may introduce more complicated effects.

4.1 Further Interactions

In this work we only considered ^{13}C impurity scattering, and disregarded all other kinds of scattering events. The objective of this approach was to obtain the characteristic lifetimes associated with the ^{13}C impurity. In this way it is possible to compare the effect of this particular scattering process with all other competing processes to determine the relative importance of each. We compared our results for the ^{13}C isotopic impurity scattering process with previously calculated values of the electron-phonon interaction which is an important process when considering optical phonons modes and their effect on the Raman spectra. Another potentially important term is the inclusion of anharmonic effects, which are associated with the thermal expansion of the lattice and such effects are observable through temperature dependent Raman spectroscopy studies [68], included in molecular dynamics simulations and

are also important in phonon transport [69], which will be a future work. Because of the temperature dependence of the anharmonic terms, such effects can in principle be tuned and accounted for in an experiment. In addition, inclusion of other types of defects like vacancies, grain boundaries, dislocations, etc. is also necessary, and understanding the relative importance of each of these scattering processes on the phonon modes as a function of temperature and other parameters remains to be investigated both theoretically and experimentally. In principle, static point defects such as substitutional atoms can be studied using a similar approach as the one used in this thesis, while extended defects such as grain boundaries or dislocations require a different treatment.

4.2 Future Work

There are still many issues for further study. Even though there has been a considerable amount of work done related to electron-phonon coupling, inclusion of anharmonic effects and phonon-defect interactions are also important for understanding the phonon-related processes in Raman spectroscopy [70] and in phonon transport more generally. Additionally, using similar procedures, this work can be extended to study the interaction of electrons with defects. In particular, substitutional defects, vacancies, grain boundaries and edges may make an important contribution to the overall phonon and electron scattering processes. Calculating the relative importance of these interactions in the full parameter space as well as understanding the signatures of defects in the Raman spectra would produce results relevant not only for basic science but also for technological applications.

Bibliography

[1] A. Jorio, M. S. Dresselhaus, R. Saito, and G. Dresselhaus. *Raman Spectroscopy in Graphene Related Systems*. Wiley-VCH, Weinheim, Germany, 2011.

[2] J. F. Rodriguez-Nieva, R. Saito, S. D. Costa, and M. S. Dresselhaus. Effect of ^{13}C isotope doping on the optical phonon modes in graphene: Localization and raman spectroscopy. *Phys. Rev. B*, 85:245406, 2012.

[3] S. D. Costa, C. Fantini, A. Righi, A. Bachmatiuk, M. H. Rümmeli, R. Saito, and M. A. Pimenta. Resonant raman spectroscopy on enriched 13C carbon nanotubes. *Carbon*, 49(14):4719 – 4723, 2011.

[4] R. A. Jishi, L. Venkataraman, M. S. Dresselhaus, and G. Dresselhaus. Phonon modes in carbon nanotubules. *Chemical Physics Letters*, 209(1-2):77 – 82, 1993.

[5] K. S. Novoselov, A. K. Geim, S. V. Morozov, D. Jiang, Y. Zhang, S. V. Dubonos, I. V. Grigorieva, and A. A. Firsov. Electric field effect in atomically thin carbon films. *Science*, 306(5696):666–669, 2004.

[6] Yu-Ming Lin, Keith A. Jenkins, Alberto Valdes-Garcia, Joshua P. Small, Damon B. Farmer, and Phaedon Avouris. Operation of graphene transistors at gigahertz frequencies. *Nano Letters*, 9(1):422–426, 2009.

[7] Lei Liao, Yung-Chen Lin, Mingqiang Bao, Rui Cheng, Jingwei Bai, Yuan Liu, Yongquan Qu, Kang L. Wang, Yu Huang, and Xiangfeng Duan. High-speed graphene transistors with a self-aligned nanowire gate. *Nature*, 467(305), 2010.

[8] F. Schedin, A. K. Geim, S. V. Morozov, E. W. Hill, P. Blake, M. I. Katsnelson, and K. S. Novoselov. Detection of individual gas molecules adsorbed on graphene. *Nat. Mat.*, 6:652–655, 2007.

[9] Paul E. Sheehan and Lloyd J. Whitman. Detection limits for nanoscale biosensors. *Nano Letters*, 5(4):803–807, 2005.

[10] Ganhua Lu, Leonidas E. Ocola, and Junhong Chen. Gas detection using low-temperature reduced graphene oxide sheets. *Applied Physics Letters*, 94(8):083111, 2009.

[11] Xuan Wang, Linjie Zhi, and Klaus Mullen. Transparent, conductive graphene electrodes for dye-sensitized solar cells. *Nano Letters*, 8(1):323–327, 2008.

[12] Shanshan Chen, Lola Brown, Mark Levendorf, Weiwei Cai, Sang-Yong Ju, Jonathan Edgeworth, Xuesong Li, Carl W. Magnuson, Aruna Velamakanni, Richard D. Piner, Junyong Kang, Jiwoong Park, and Rodney S. Ruoff. Oxidation resistance of graphene-coated Cu and Cu/Ni alloy. *ACS Nano*, 5(2):1321–1327, 2011.

[13] M. Endo, S. Iijima, and M. S. Dresselhaus. *Carbon Nanotubes*. Pergamon, Oxford; Tarrytown, N. Y., 1996.

[14] T. Natsuki, K. Tantrakarn, and M. Endo. Effects of carbon nanotube structures on mechanical properties. *Applied Physics A: Materials Science & Processing*, 79:117–124, 2004.

[15] Alain Peigney. Composite materials: Tougher ceramics with nanotubes. *Nat Mater*, 2(1):15–16, 2003.

[16] N. D. Mermin and H. Wagner. Absence of ferromagnetism or antiferromagnetism in one- or two-dimensional isotropic heisenberg models. *Phys. Rev. Lett.*, 17:1133–1136, 1966.

[17] Oleg V. Yazyev and Steven G. Louie. Topological defects in graphene: Dislocations and grain boundaries. *Phys. Rev. B*, 81:195420, 2010.

[18] Claire Berger, Zhimin Song, Xuebin Li, Xiaosong Wu, Nate Brown, Ccile Naud, Didier Mayou, Tianbo Li, Joanna Hass, Alexei N. Marchenkov, Edward H. Conrad, Phillip N. First, and Walt A. de Heer. Electronic confinement and coherence in patterned epitaxial graphene. *Science*, 312(5777):1191–1196, 2006.

[19] V. P. Gusynin and S. G. Sharapov. Unconventional integer quantum hall effect in graphene. *Phys. Rev. Lett.*, 95:146801, 2005.

[20] Xinxin Yu, Hongbing Cai, Wenhua Zhang, Xinjing Li, Nan Pan, Yi Luo, Xiaoping Wang, and J. G. Hou. Tuning chemical enhancement of sers by controlling the chemical reduction of graphene oxide nanosheets. *ACS Nano*, 5(2):952–958, 2011.

[21] Elizabeth S. Thrall, Andrew C. Crowther, Zhonghua Yu, and Louis E. Brus. R6g on graphene: High raman detection sensitivity, yet decreased raman cross-section. *Nano Letters*, 12(3):1571–1577, 2012.

[22] Nikolaos Tombros, Csaba Jozsa, Mihaita Popinciuc, Harry T. Jonkman, and Bart J. van Wees. Electronic spin transport and spin precession in single graphene layers at room temperature. *Nature*, 448:571–574, 2007.

[23] Alexander A. Balandin, Suchismita Ghosh, Wenzhong Bao, Irene Calizo, Desalegne Teweldebrhan, Feng Miao, and Chun Ning Lau. Superior thermal conductivity of single-layer graphene. *Nano Letters*, 8(3):902–907, 2008. PMID: 18284217.

[24] Changgu Lee, Xiaoding Wei, Jeffrey W. Kysar, and James Hone. Measurement of the elastic properties and intrinsic strength of monolayer graphene. *Science*, 321(5887):385–388, 2008.

[25] A. K. Geim and K. S. Novoselov. The rise of graphene. *Nat Mater*, 6(3):183–191, 2007.

[26] E. H. Hwang, S. Adam, and S. Das Sarma. Carrier transport in two-dimensional graphene layers. *Phys. Rev. Lett.*, 98:186806, May 2007.

[27] John R. Miller, R. A. Outlaw, and B. C. Holloway. Graphene double-layer capacitor with ac line-filtering performance. *Science*, 329(5999):1637–1639, 2010.

[28] Dmitry V. Kosynkin, Amanda L. Higginbotham, Jay R. Sinitskii, Alexander Lomeda, Ayrat Dimiev, B. Katherine Price, and James M. Tour. Longitudinal unzipping of carbon nanotubes to form graphene nanoribbons. *Nature*, 458:872–876, 2009.

[29] Kyoko Nakada, Mitsutaka Fujita, Gene Dresselhaus, and Mildred S. Dresselhaus. Edge state in graphene ribbons: Nanometer size effect and edge shape dependence. *Phys. Rev. B*, 54:17954–17961, 1996.

[30] Mitsutaka Fujita, Katsunori Wakabayashi, Kyoko Nakada, and Koichi Kusakabe. Peculiar localized state at zigzag graphite edge. *Journal of the Physical Society of Japan*, 65(7):1920–1923, 1996.

[31] Young-Woo Son, Marvin L. Cohen, and Steven G. Louie. Energy gaps in graphene nanoribbons. *Phys. Rev. Lett.*, 97:216803, 2006.

[32] O. Lehtinen, J. Kotakoski, A. V. Krasheninnikov, A. Tolvanen, K. Nordlund, and J. Keinonen. Effects of ion bombardment on a two-dimensional target: Atomistic simulations of graphene irradiation. *Phys. Rev. B*, 81:153401, 2010.

[33] Humberto Terrones, Ruitao Lv, Mauricio Terrones, and Mildred S Dresselhaus. The role of defects and doping in 2d graphene sheets and 1d nanoribbons. *Reports on Progress in Physics*, 75(6):062501, 2012.

[34] A.J. Stone and D.J. Wales. Theoretical studies of icosahedral C60 and some related species. *Chemical Physics Letters*, 128(56):501 – 503, 1986.

[35] H. Terrones, M. Terrones, E. Hernández, N. Grobert, J-C. Charlier, and P. M. Ajayan. New metallic allotropes of planar and tubular carbon. *Phys. Rev. Lett.*, 84:1716–1719, 2000.

[36] Masahiro Morooka, Takahiro Yamamoto, and Kazuyuki Watanabe. Defect-induced circulating thermal current in graphene with nanosized width. *Phys. Rev. B*, 77:033412, 2008.

[37] D. W. Boukhvalov and M. I. Katsnelson. Chemical functionalization of graphene with defects. *Nano Letters*, 8(12):4373–4379, 2008.

[38] Bing Huang, Miao Liu, Ninghai Su, Jian Wu, Wenhui Duan, Bing-lin Gu, and Feng Liu. Quantum manifestations of graphene edge stress and edge instability: A first-principles study. *Phys. Rev. Lett.*, 102:166404, 2009.

[39] H. Amara, S. Latil, V. Meunier, Ph. Lambin, and J.-C. Charlier. Scanning tunneling microscopy fingerprints of point defects in graphene: A theoretical prediction. *Phys. Rev. B*, 76:115423, 2007.

[40] Zuanyi Li, Haiyun Qian, Jian Wu, Bing-Lin Gu, and Wenhui Duan. Role of symmetry in the transport properties of graphene nanoribbons under bias. *Phys. Rev. Lett.*, 100:206802, 2008.

[41] Yun Ren and Ke-Qiu Chen. Effects of symmetry and stone–wales defect on spin-dependent electronic transport in zigzag graphene nanoribbons. *Journal of Applied Physics*, 107(4):044514, 2010.

[42] F. Cervantes-Sodi, G. Csányi, S. Piscanec, and A. C. Ferrari. Edge-functionalized and substitutionally doped graphene nanoribbons: Electronic and spin properties. *Phys. Rev. B*, 77:165427, 2008.

[43] B. Huang. *Phys. Lett. A*, 375:845, 2011.

[44] Elham Beheshti, Alireza Nojeh, and Peyman Servati. A first-principles study of calcium-decorated, boron-doped graphene for high capacity hydrogen storage. *Carbon*, 49(5):1561 – 1567, 2011.

[45] Pablo A. Denis, Ricardo Faccio, and Alvaro W. Mombru. Is it possible to dope single-walled carbon nanotubes and graphene with sulfur? *ChemPhysChem*, 10(4):715–722, 2009.

[46] Y. Zou, F. Li, Z. H. Zhu, M. W. Zhao, X. G. Xu, and X. Y. Su. An ab initio study on gas sensing properties of graphene and si-doped graphene. *Eur. Phys. J. B*, 81(475), 2011.

[47] Shanshan Chen, Qingzhi Wu, Columbia Mishra, Junyong Kang, Hengji Zhang, Kyeongjae Cho, Weiwei Cai, Alexander A. Balandin, and Rodney S. Ruoff. Thermal conductivity of isotopically modified graphene. *Nat Mater*, 2012.

[48] Y. Miyauchi and S. Maruyama. Identification of an excitonic phonon sideband by photoluminescence spectroscopy of single-walled carbon-13 nanotubes. *Phys. Rev. B*, 74:035415, 2006.

[49] S. Fan, L. Liu, and M. Liu. Monitoring the growth of carbon nanotubes by carbon isotope labelling. *Nanotechnology*, 14(10):1118, 2003.

[50] X. Li, W. Cai, L. Colombo, and R. S. Ruoff. Evolution of graphene growth on Ni and Cu by carbon isotope labeling. *Nano Letters*, 9(12):4268–4272, 2009.

[51] M. Kalbac, H. Farhat, J. Kong, P. Janda, L. Kavan, and M. S. Dresselhaus. Raman spectroscopy and in situ raman spectroelectrochemistry of bilayer 12C/13C graphene. *Nano Letters*, 11(5):1957–1963, 2011.

[52] Martin Kalbac, Otakar Frank, Jing Kong, Javier Sanchez-Yamagishi, Kenji Watanabe, Takashi Taniguchi, Pablo Jarillo-Herrero, and Mildred S. Dresselhaus. Large variations of the raman signal in the spectra of twisted bilayer graphene on a bn substrate. *The Journal of Physical Chemistry Letters*, 3(6):796–799, 2012.

[53] I. Savić, N. Mingo, and D. A. Stewart. Phonon transport in isotope-disordered carbon and boron-nitride nanotubes: Is localization observable? *Phys. Rev. Lett.*, 101:165502, 2008.

[54] T. Yamamoto, K. Sasaoka, and S. Watanabe. Universality and diversity in a phonon-transmission histogram of isotope-disordered carbon nanotubes. *Phys. Rev. Lett.*, 106:215503, 2011.

[55] P. W. Anderson. Absence of diffusion in certain random lattices. *Phys. Rev.*, 109:1492–1505, 1958.

[56] B. Kramer and A. MacKinnon. Localization: theory and experiment. *Reports on Progress in Physics*, 56(12):1469, 1993.

[57] D. S. Wiersma, P. Bartolini, A. Lagendijk, and R. Righini. Localization of light in a disordered medium. *Nature*, 390:671–673, 1997.

[58] P. E. Lindelof, J. Nørregaard, and J. Hanberg. New light on the scattering mechanisms in Si inversion layers by weak localization experiments. *Physica Scripta*, (T14):17, 1986.

[59] A. C. Ferrari. Raman spectroscopy of graphene and graphite: Disorder, electron-phonon coupling, doping and nonadiabatic effects. *Solid State Communications*, 143(1-2):47 – 57, 2007.

[60] A. H. Castro Neto and F. Guinea. Electron-phonon coupling and raman spectroscopy in graphene. *Phys. Rev. B*, 75:045404, 2007.

[61] E. B. Barros, K. Sato, Ge. G. Samsonidze, A. G. Souza Filho, M. S. Dresselhaus, and R. Saito. *D* band raman intensity calculation in armchair edged graphene nanoribbons. *Phys. Rev. B*, 83:245435, 2011.

[62] F. Wegner. Inverse participation ratio in $2+\epsilon$ dimensions. *Zeitschrift für Physik B Condensed Matter*, 36:209–214, 1980.

[63] P. G. Klemens. The scattering of low-frequency lattice waves by static imperfections. *Proceedings of the Physical Society. Section A*, 68(12):1113, 1955.

[64] L. Lindsay, D. A. Broido, and Natalio Mingo. Flexural phonons and thermal transport in multilayer graphene and graphite. *Phys. Rev. B*, 83:235428, 2011.

[65] J. Jiang, R. Saito, A. Grüneis, G. Dresselhaus, and M.S. Dresselhaus. Electron-phonon interaction and relaxation time in graphite. *Chemical Physics Letters*, 392(46):383 – 389, 2004.

[66] J. Jiang, R. Saito, Ge. G. Samsonidze, S. G. Chou, A. Jorio, G. Dresselhaus, and M. S. Dresselhaus. Electron-phonon matrix elements in single-wall carbon nanotubes. *Phys. Rev. B*, 72:235408, 2005.

[67] J. M. Ziman. *Models of disorder : the theoretical physics of homogeneously disordered systems.* Cambridge University Press, Cambridge, 1979.

[68] I. Calizo, A. A. Balandin, W. Bao, F. Miao, and C. N. Lau. Temperature dependence of the raman spectra of graphene and graphene multilayers. *Nano Letters*, 7(9):2645–2649, 2007.

[69] L. Lindsay, D. A. Broido, and N. Mingo. Flexural phonons and thermal transport in graphene. *Phys. Rev. B*, 82:115427, 2010.

[70] P. Venezuela, M. Lazzeri, and F. Mauri. Theory of double-resonant raman spectra in graphene: Intensity and line shape of defect-induced and two-phonon bands. *Phys. Rev. B*, 84:035433, 2011.